

Computational Science Laboratory
Report CSL-TR-20-6
November 6, 2020

Steven Roberts, Andrey A. Popov, Arash
Sarshar, and Adrian Sandu

*“A fast time-stepping strategy for ODE
systems equipped with a surrogate model”*

Computational Science Laboratory
“Compute the Future!”

Department of Computer Science
Virginia Polytechnic Institute and State University
Blacksburg, VA 24060
Phone: (540)-231-2193
Fax: (540)-231-6075
Email: steven94@vt.edu, apopov@vt.edu, sarshar@vt.edu,
sandu@cs.vt.edu
Web: <http://cs1.cs.vt.edu>



A FAST TIME-STEPPING STRATEGY FOR ODE SYSTEMS EQUIPPED WITH A SURROGATE MODEL*

STEVEN ROBERTS[†], ANDREY A POPOV[†], ARASH SARSHAR[†], AND ADRIAN SANDU[†]

Abstract. Simulation of complex dynamical systems arising in many applications is computationally challenging due to their size and complexity. Model order reduction, machine learning, and other types of surrogate modeling techniques offer cheaper and simpler ways to describe the dynamics of these systems, but are inexact and introduce additional approximation errors. In order to overcome the computational difficulties of the full complex models, on one hand, and the limitations of surrogate models, on the other, this work proposes a new accelerated time-stepping strategy that combines information from both. This approach is based on the multirate infinitesimal general-structure additive Runge–Kutta (MRI-GARK) framework. The inexpensive surrogate model is integrated with a small timestep to guide the solution trajectory, and the full model is treated with a large timestep to occasionally correct for the surrogate model error and ensure convergence. We provide a theoretical error analysis, and several numerical experiments, to show that this approach can be significantly more efficient than using only the full or only the surrogate model for the integration.

Key words. Multirate time integration, Surrogate model, General-structure additive Runge–Kutta methods, Reduced order modeling, Machine learning

AMS subject classifications. 65L05, 65F99

1. Introduction. This paper will consider the system of ordinary differential equations (ODEs)

$$(1.1) \quad y' = f(t, y), \quad y(t_0) = y_0, \quad y \in \mathbb{C}^N,$$

equipped with a surrogate model approximating the dynamics of (1.1):

$$(1.2) \quad y'_s = f_s(t, y_s), \quad y_s \in \mathbb{C}^S.$$

This surrogate model is assumed to be much less expensive to solve than the full model (1.1), possibly by evolving in a lower dimensional space ($S < N$). Moreover, we assume that projections between the full and surrogate model spaces are realized by the matrices $V, W \in \mathbb{C}^{N \times S}$:

$$(1.3) \quad y_s = W^* y, \quad y \approx V y_s, \quad W^* V = I_{S \times S}.$$

Here, the $*$ symbol denotes the conjugate transpose of a matrix.

This paper presents a new technique to supplement the numerical integration of (1.1) using the surrogate model (1.2). For an appropriate choice of surrogate model, our method can be significantly more efficient than using either the full or the surrogate model alone. This is accomplished by applying a multirate time integration scheme to the additively partitioned ODE

$$(1.4) \quad y' = \underbrace{V f_s(t, W^* y)}_{f^{\{\dagger\}}(t, y)} + \underbrace{f(t, y) - V f_s(t, W^* y)}_{f^{\{\circ\}}(t, y)}.$$

*Submitted to the editors DATE.

Funding: TODO

[†]Computational Science Laboratory, Virginia Polytechnic Institute and State University, Blacksburg, VA 24060 (steven94@vt.edu, apopov@vt.edu, sarshar@vt.edu, sandu@cs.vt.edu).

Multirate methods are characterized by using different stepsizes for different parts of an ODE, as opposed to a single, global timestep [2, 10, 11, 19, 20, 23, 42, 50, 51]. For problems with partitions exhibiting vastly different time scales, stiffnesses, evaluation costs, or amounts of nonlinearity, multirate methods can be more efficient than their single rate counterparts. In (1.4), there are two partitions: a fast partition $f^{\{f\}}$ which is treated with a small timestep and a slow partition $f^{\{s\}}$ which is treated with a large timestep. Note that (1.4) has the same solution as (1.1). It is rewritten and partitioned, however, in such a way that $f^{\{f\}}$ contains the surrogate model dynamics and $f^{\{s\}}$ represents the error in the surrogate model. Ideally, this error will be small, so a large timestep would be acceptable. Moreover, this means expensive evaluations of the full model occur infrequently compared to the inexpensive surrogate model evaluations.

With about 60 years of development [42], the multirating strategy has been applied to numerous classes of time integration methods. Conceivably any multirate method suitable for additively partitioned systems could be applied to (1.4). This paper builds upon multirate infinitesimal methods [5, 29, 53, 57], as they offer a particularly flexible and elegant approach to multirate integration. In particular, we use the multirate infinitesimal general-structure additive Runge–Kutta (MRI-GARK) framework proposed in [45, 49]. MRI-GARK is an appealing choice as it generalizes many types of multirate infinitesimal methods, allows for the construction of high order methods, and supports implicit stages. We note, however, that this paper primarily focuses on explicit methods where (1.1) is nonstiff.

There are other instances in the literature where multirate methods and surrogate models are used in conjunction. In [24], an implicit multirate scheme is used to simulate a fast-evolving electric circuit coupled with a slow-evolving electric field. Model order reduction is then applied to the electric field problem to further reduce the computational cost. A multirate Runge–Kutta–Chebyshev method is proposed in [1] using a time-averaged right hand side, which can be viewed as a surrogate model with better stiffness properties. Also related are high-order/low-order (HOLO) methods [8] for systems of nonlinear equations where a high-complexity model is coupled with a low-complexity model. HOLO is based on nonlinear elimination [30], and has the computationally appealing property that nonlinear solves are performed in a low-dimensional space. Finally, surrogate models have been used extensively to speed up optimization problems when objective function evaluations are expensive [13, 34, 37].

This remainder of this paper is structured as follows. In section 2, we review the MRI-GARK framework and extensions. Section 3 then specializes MRI-GARK-type methods to the special ODE (1.4). An error analysis is performed in section 4, and various approaches for constructing surrogate models are discussed in section 5. Convergence and performance experiments can be found in section 6. Finally, section 7 summarizes the results of the paper and proposes future extensions.

2. Multirate infinitesimal general-structure additive Runge–Kutta methods. In this section, we will briefly review the MRI-GARK framework, as it serves as the foundation for the remainder of the paper. These methods numerically solve ODEs that are additively partitioned into fast and slow dynamics:

$$(2.1) \quad y' = f^{\{f\}}(y) + f^{\{s\}}(y).$$

The defining characteristic of multirate infinitesimal methods is that the slow dynamics $f^{\{s\}}$ is propagated with a discrete method, most commonly a Runge–Kutta method, while the fast dynamics $f^{\{f\}}$ is propagated continuously through modified

fast ODEs. An MRI-GARK scheme [49] advances the solution of (2.1) from time t_n to $t_{n+1} = t_n + H$ via the following computational process:

$$\begin{aligned}
 (2.2a) \quad & Y_1^{\{s\}} = y_n, \\
 (2.2b) \quad & \begin{cases} v_i(0) = Y_i^{\{s\}}, \\ T_i = t_n + c_i^{\{s\}} H, \\ v'_i(\theta) = \Delta c_i^{\{s\}} f^{\{f\}}(T_i + \Delta c_i^{\{s\}} \theta, v_i(\theta)) + \sum_{j=1}^{i+1} \gamma_{i,j}(\frac{\theta}{H}) f^{\{s\}}(T_j, Y_j^{\{s\}}), \\ \text{for } \theta \in [0, H], \\ Y_{i+1}^{\{s\}} = v_i(H), \quad i = 1, \dots, s^{\{s\}}, \end{cases} \\
 (2.2c) \quad & y_{n+1} = Y_{s^{\{s\}}+1}^{\{s\}}.
 \end{aligned}$$

There are $s^{\{s\}}$ modified fast ODEs (2.2b) solved between the abscissae of a Runge–Kutta method. The distances between consecutive abscissae are

$$\Delta c_i^{\{s\}} = \begin{cases} c_{i+1}^{\{s\}} - c_i^{\{s\}}, & i = 1, \dots, s^{\{s\}} - 1, \\ 1 - c_{s^{\{s\}}}^{\{s\}}, & i = s^{\{s\}}. \end{cases}$$

Equation (2.2b) also contains time-dependent, polynomial forcing terms for the slow dynamics which satisfy

$$(2.3) \quad \gamma_{i,j}(t) := \sum_{k \geq 0} \gamma_{i,j}^k t^k, \quad \tilde{\gamma}_{i,j}(t) := \int_0^t \gamma_{i,j}(\tau) d\tau = \sum_{k \geq 0} \gamma_{i,j}^k \frac{t^{k+1}}{k+1}, \quad \bar{\gamma}_{i,j} := \tilde{\gamma}_{i,j}(1).$$

Continuing with the notation of [49], capitalized versions of (2.3) denote matrices of coefficients. If $\bar{\Gamma}$ is lower triangular, (2.2) is explicit, and otherwise, it is implicit.

For general $f^{\{f\}}$ one cannot expect to find a closed-form solution to the modified fast ODE (2.2b); however by time-stepping it with an “infinitesimally” small timestep, one can determine $v_i(H)$ exactly. For purposes of computational practicality, the infinitesimally small timestep is loosened to a timestep small enough that fast solution errors are negligible. Multirate infinitesimal methods enjoy great flexibility in that *any* consistent time integration method can be used to solve the modified fast ODE provided sufficiently many steps are taken. This offers the freedom to choose implicit or explicit methods, as well as methods of any order. Equation (2.2) is multirate in the sense that there are $s^{\{s\}}$ evaluations of $f^{\{s\}}$ over a timestep H , while (2.2b) is generally integrated with a much smaller timestep and requires many more evaluations of $f^{\{f\}}$.

2.1. Coupled MRI-GARK schemes. In [44] two new types of MRI-GARK methods were proposed: step predictor-corrector MRI-GARK (SPC-MRI-GARK) and internal predictor-corrector MRI-GARK (IPC-MRI-GARK). In order to improve the linear stability of MRI-GARK, both include coupled, discrete prediction stages that are subsequently corrected by solving modified fast ODEs. In comparing the two MRI-GARK variants, SPC-MRI-GARK was identified to have simpler order conditions, better stability, and a simpler implementation. For these reasons, we will only consider SPC-MRI-GARK in the construction of surrogate model timestepping techniques.

An SPC-MRI-GARK method based on the “slow” Runge–Kutta method $(\mathcal{A}^{\{s\}}, \mathcal{b}^{\{s\}}, c^{\{s\}})$ solves (2.1) with steps of the form:

$$(2.4a) \quad Y_i = y_n + H \sum_{j=1}^{s^{\{s\}}} a_{i,j}^{\{s\}} f(t_n + c_j^{\{s\}} H, Y_j), \quad i = 1, \dots, s^{\{s\}},$$

$$(2.4b) \quad \begin{cases} v(0) = y_n, \\ v' = f^{\{f\}}(t_n + \theta, v) + \sum_{j=1}^{s^{\{s\}}} \gamma_j\left(\frac{\theta}{H}\right) f^{\{s\}}(t_n + c_j^{\{s\}} H, Y_j), & \text{for } \theta \in [0, H], \\ y_{n+1} = v(H). \end{cases}$$

Similar to a traditional Runge–Kutta scheme, SPC-MRI-GARK starts by computing stage values that approximate the solution at the times $t_n + c_i^{\{s\}} H$. In this prediction step (2.4a), the fast and slow dynamics are treated together with the timestep H . The fast part of the stage values is inaccurate from this large timestep and is discarded. A single ODE (2.4b) is solved from t_n to t_{n+1} to correct the fast dynamics and produce the next step y_{n+1} . Like MRI-GARK, there are time-dependent, polynomial forcing terms for the slow tendencies. Following [44, Definition 2.2], the definitions of $\gamma_i(t)$, $\tilde{\gamma}_i(t)$, $\bar{\gamma}_i$ are identical to (2.3), except they are vector quantities with a single subscript index. While base methods of any structure are admitted in the SPC-MRI-GARK framework, only diagonally implicit methods were considered in [44]. As the focus of this paper is explicit methods, we have derived new explicit methods of orders two and three and present their coefficients in Appendix A.

3. Method formulation. Following the process outlined in the introduction, we seek to apply the MRI-GARK method (2.2) to the partitioned problem (1.4) in order to construct a solution process that can incorporate surrogate model information. We start with the modified fast ODE (2.2b):

$$(3.1) \quad \begin{aligned} v'_i(\theta) &= \Delta c_i^{\{s\}} V f_s\left(T_i + \Delta c_i^{\{s\}} \theta, W^* v_i(\theta)\right) \\ &+ \sum_{j=1}^{i+1} \gamma_{i,j}\left(\frac{\theta}{H}\right) (f(T_j, Y_j) - V f_s(T_j, W^* Y_j)). \end{aligned}$$

In (3.1) the full model f only appears in the forcing terms, and for explicit methods, it is evaluated at previously computed stage values. Only the surrogate model f_s needs to be evaluated at each of the infinitesimal steps to compute $v_i(H)$.

Note that in formulation (3.1) $v_i \in \mathbb{C}^N$ evolve in the full space, and there is no benefit from choosing a surrogate model that evolves in a lower dimensional space. To fix this, we first split v_i into the parts residing inside and outside the surrogate model space:

$$v_i(\theta) = VW^* v_i(\theta) + (I_{N \times N} - VW^*) v_i(\theta).$$

More formally, VW^* and $(I_{N \times N} - VW^*)$ define oblique projections onto the range of V and the nullspace of W^* , respectively. We now consider the solution to (3.1) from the perspective of these two, complementary subspaces.

Starting outside the surrogate model space, we have that

$$\begin{aligned}
 (I_{N \times N} - VW^*) v_i(H) &= (I_{N \times N} - VW^*) \left(Y_i + \int_0^H v_i'(\theta) d\theta \right) \\
 (3.2) \quad &= (I_{N \times N} - VW^*) \left(Y_i + H \sum_{j=1}^i \bar{\gamma}_{i,j} f(T_j, Y_j) \right),
 \end{aligned}$$

where we have used (2.3) and the fact that $(I_{N \times N} - VW^*)V = 0_{N \times S}$ by (1.3). Equation (3.2) reveals that inside the nullspace of W^* the solution equation (3.1) becomes a Runge–Kutta stage. Therefore, we exclude the components in this subspace during the infinitesimal step integration of (3.1).

We now consider the dynamics (3.1) projected onto the surrogate model space:

$$\begin{aligned}
 (3.3) \quad z_i(\theta) &:= W^* v_i(\theta) \in \mathbb{C}^S, \\
 z_i'(\theta) &= \Delta c_i^{\{s\}} f_s \left(T_i + \Delta c_i^{\{s\}} \theta, z_i(\theta) \right) + \sum_{j=1}^{i+1} \gamma_{i,j} \left(\frac{\theta}{H} \right) (W^* f(T_j, Y_j) - f_s(T_j, W^* Y_j)).
 \end{aligned}$$

The solution to (3.1) can be expressed as the sum of its two components:

$$v_i(H) = Vz_i(H) + (I_{N \times N} - VW^*) \left(Y_i + H \sum_{j=1}^{i+1} \bar{\gamma}_{i,j} f(T_j, Y_j) \right).$$

Thus to compute an MRI-GARK stage, we only need to solve an ODE of dimension S instead of N . We summarize the simplifications of (2.2) in Definition 3.1 and provide a graphical illustration in Figure 1.

DEFINITION 3.1 (SM-MRI-GARK). *A surrogate model MRI-GARK (SM-MRI-GARK) method solves the ODE (1.1) with the help of the surrogate model (1.2) using steps of the form*

$$(3.4a) \quad Y_1 = y_n,$$

$$(3.4b) \quad \left\{ \begin{aligned} &z_i(0) = W^* Y_i, \\ &T_i = t_n + c_i^{\{s\}} H, \\ &z_i'(\theta) = \Delta c_i^{\{s\}} f_s \left(T_i + \Delta c_i^{\{s\}} \theta, z_i(\theta) \right) \\ &\quad + \sum_{j=1}^{i+1} \gamma_{i,j} \left(\frac{\theta}{H} \right) (W^* f(T_j, Y_j) - f_s(T_j, W^* Y_j)), \quad \text{for } \theta \in [0, H], \\ &Y_{i+1} = Vz_i(H) + (I_{d \times d} - VW^*) \left(Y_i + H \sum_{j=1}^{i+1} \bar{\gamma}_{i,j} f(T_j, Y_j) \right), \\ &i = 1, \dots, s^{\{s\}}, \end{aligned} \right.$$

$$(3.4c) \quad y_{n+1} = Y_{s^{\{s\}}+1}.$$

Remark 3.2 (Telescopic SM-MRI-GARK for hierarchical surrogate models). For certain applications an entire hierarchy surrogate models $f, f_s^1, f_s^2, \dots, f_s^m$, may be

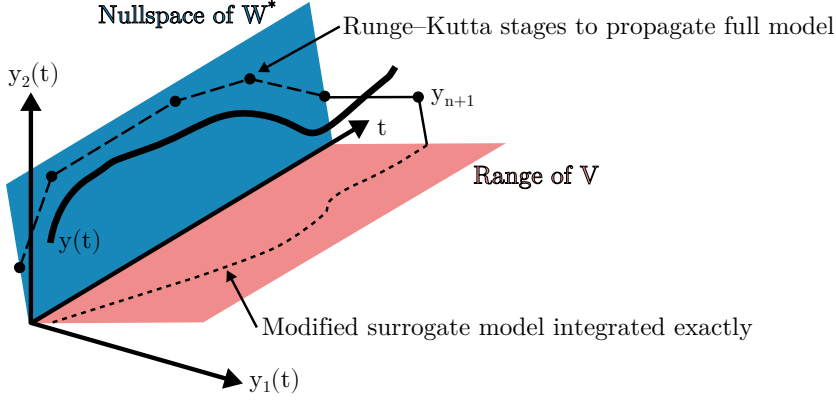


Fig. 1: Illustration of SM-MRI-GARK for a two-variable ODE and a surrogate model that evolves in a one-dimensional subspace.

available. In such scenarios, one can take advantage of all models by applying SM-MRI-GARK recursively. First, the highest fidelity models f and f_s^1 are applied to (3.4). The ODE (3.4b), is then solved using an SM-MRI-GARK method with $\Delta c_i^{\{s\}} f_s^2$ as the surrogate model. Its ODEs are solved using an SM-MRI-GARK method with $\Delta c_i^{\{s\} \times 2} f_s^3$ as the surrogate model. This is continued until we reach $\Delta c_i^{\{s\} \times (m-1)} f_s^m$ as the lowest fidelity surrogate model. Note the power of $\Delta c_i^{\{s\}}$ scaling the surrogate models can be eliminated by applying the change of variable $\theta \rightarrow \theta / \Delta c_i^{\{s\}}$ to (3.4b).

Remark 3.3 (Connection to EPRIRK-K methods). In [49], Sandu showed that exponential Runge-Kutta methods are special case of MRI-GARK methods when the linear-nonlinear partitioning

$$(3.5) \quad y' = \underbrace{Ly}_{f^{\{l\}}} + \underbrace{f(t, y) - Ly}_{f^{\{s\}}}$$

is used. Conversely, MRI-GARK can be viewed as a generalization of exponential Runge-Kutta methods where the piece integrated exactly can be linear or nonlinear.

An analogous connection can be made between EPIRK-K [33] and SM-MRI-GARK. EPIRK-K is an extension of exponential propagation iterative methods of Runge-Kutta type (EPIRK) [56] that approximates the Jacobian $J_n = f_y(t_n, y_n)$ appearing in matrix exponentials and related matrix functions with a Krylov-subspace approximation $UU^*J_nUU^*$. SM-MRI-GARK with $V = W = U$ and $f_s(t, y_s) = U^*J_nUy_s$ recovers the full class of EPIRK-K schemes.

As a simple example of an SM-MRI-GARK method, consider forward Euler as the base method and the internally consistent [49, Section 3.1.1] coupling $\gamma_{1,1}(t) = 1$:

$$(3.6) \quad \begin{aligned} z(0) &= W^*y_n \\ z'(\theta) &= f_s(t_n + \theta, z(\theta)) + W^*f(t_n, y_n) - f_s(t_n, W^*y_n), \quad \text{for } \theta \in [0, H], \\ y_{n+1} &= Vz(H) + (I_{d \times d} - VW^*)(y_n + Hf(t_n, y_n)). \end{aligned}$$

Equation (3.6) is only first order accurate; however, second and third order SM-MRI-GARK schemes can be constructed using the coefficients provided in Appendix A. In

order to implement these efficiently, we have provided pseudocode in [Algorithm 3.1](#). It minimizes the number of full and surrogate model evaluations, as well as the number of matrix-vector products involving V and W^* .

Algorithm 3.1 Pseudocode for explicit SM-MRI-GARK [\(3.4\)](#).

```

1: procedure SM-MRI-GARK( $f, f_s, V, W^*, t_0, t_{\text{end}}, y_0, N_{\text{steps}}$ )
2:    $y = y_0$ 
3:    $\hat{y} = W^* y_0$ 
4:    $H = (t_{\text{end}} - t_0) / N_{\text{steps}}$ 
5:   for  $n = 1, \dots, N_{\text{steps}}$  do
6:     for  $i = 1, \dots, s^{\{\mathbf{s}\}}$  do
7:        $T_i = t_0 + \left(n + c_i^{\{\mathbf{s}\}}\right) H$ 
8:        $k_i = f(T_i, y)$ 
9:        $\hat{k}_i = W^* k_i$ 
10:       $\hat{\ell}_i = \hat{k}_i - f_s(T_i, \hat{y})$ 
11:       $\hat{w} = \hat{y} + H \sum_{j=1}^i \bar{\gamma}_{i,j} \hat{k}_j$ 
12:       $y = y + H \sum_{j=1}^i \bar{\gamma}_{i,j} k_j$ 
13:       $\hat{y} = \text{OdeSolve}\left(z'_i(\theta) = \Delta c_i^{\{\mathbf{s}\}} f_s\left(T_i + \Delta c_i^{\{\mathbf{s}\}} \theta, z_i(\theta)\right) + \sum_{j=1}^i \gamma_{i,j}\left(\frac{\theta}{H}\right) \hat{\ell}_j,\right.$ 
         $\left. \text{timespan} = [0, H], \text{initial\_condition} = \hat{y}\right)$ 
14:       $y = y + V(\hat{y} - \hat{w})$ 
15:     end for
16:   end for
17:   return  $y$ 
18: end procedure

```

3.1. Formulation for SPC-MRI-GARK. A similar process can be used to apply SPC-MRI-GARK [\(2.4\)](#) to the ODE [\(1.4\)](#). For brevity, we avoid replicating the simplifications [\(3.2\)](#) and [\(3.3\)](#) and directly present the method formulation in the following definition.

DEFINITION 3.4 (SM-SPC-MRI-GARK). *A surrogate model SPC-MRI-GARK (SM-SPC-MRI-GARK) method solves the ODE [\(1.1\)](#) with the help of the surrogate model [\(1.2\)](#) using steps of the form*

$$(3.7a) \quad Y_i = y_n + H \sum_{j=1}^{s^{\{\mathbf{s}\}}} a_{i,j}^{\{\mathbf{s}\}} f\left(t_n + c_j^{\{\mathbf{s}\}} H, Y_j\right), \quad i = 1, \dots, s^{\{\mathbf{s}\}},$$

$$(3.7b) \quad \left\{ \begin{array}{l} z(0) = W^* y_n, \\ z(\theta)' = f_s(t_n + \theta, z(\theta)) \\ \quad + \sum_{j=1}^{s^{\{\mathbf{s}\}}} \gamma_j\left(\frac{\theta}{H}\right) \left(W^* f(t_n + c_j^{\{\mathbf{s}\}} H, Y_j) - f_s\left(t_n + c_j^{\{\mathbf{s}\}} H, W^* Y_j\right)\right), \\ \text{for } \theta \in [0, H], \\ y_{n+1} = Vz(H) + (I_{d \times d} - VW^*) \left(y_n + H \sum_{j=1}^{s^{\{\mathbf{s}\}}} b_j f(t_n + c_j^{\{\mathbf{s}\}} H, Y_j)\right). \end{array} \right.$$

The SM-MRI-GARK Euler method from (3.6) also happens to be an SM-SPC-MRI-GARK method. The base method is again forward Euler, and the coupling is $\gamma_1(t) = 1$. Methods with more than one stage will not coincide, however, as SM-SPC-MRI-GARK has one modified fast ODE per step while SM-MRI-GARK has $s^{\{s\}}$. Another distinction, which can be seen in Algorithm 3.2, is that SM-SPC-MRI-GARK only requires one matrix-vector product with V per step, while SM-MRI-GARK requires $s^{\{s\}}$.

Algorithm 3.2 Pseudocode for explicit SM-SPC-MRI-GARK (3.7).

```

1: procedure SM-SPC-MRI-GARK( $f, f_s, V, W^*, t_0, t_{\text{end}}, y_0, N_{\text{steps}}$ )
2:    $y = y_0$ 
3:    $\hat{y} = W^* y_0$ 
4:    $H = (t_{\text{end}} - t_0) / N_{\text{steps}}$ 
5:   for  $n = 1, \dots, N_{\text{steps}}$  do
6:      $t_n = t_0 + nH$ 
7:     for  $i = 1, \dots, s^{\{s\}}$  do
8:        $k_i = f\left(t_n + c_i^{\{s\}}H, y + H \sum_{j=1}^{i-1} a_{i,j}^{\{s\}} k_j\right)$ 
9:        $\hat{k}_i = W^* k_i$ 
10:       $\hat{\ell}_i = \hat{k}_i - f_s\left(t_n + c_i^{\{s\}}H, \hat{y} + H \sum_{j=1}^{i-1} a_{i,j}^{\{s\}} \hat{k}_j\right)$ 
11:    end for
12:     $\hat{w} = \hat{y} + H \sum_{j=1}^{s^{\{s\}}} b_j^{\{s\}} \hat{k}_j$ 
13:     $y = y + H \sum_{j=1}^{s^{\{s\}}} b_j^{\{s\}} k_j$ 
14:     $\hat{y} = \text{OdeSolve}\left(z'(\theta) = f_s(t_n + \theta, z(\theta)) + \sum_{j=1}^{s^{\{s\}}} \gamma_j\left(\frac{\theta}{H}\right) \hat{\ell}_j, \right.$ 
        $\text{timespan} = [0, H], \text{initial\_condition} = \hat{y})$ 
15:     $y = y + V(\hat{y} - \hat{w})$ 
16:  end for
17:  return  $y$ 
18: end procedure

```

4. Error analysis. Consider the edge case where the surrogate model is taken to be the full model and $V = W^* = I_{N \times N}$. The stages of (3.4) simplify to

$$\begin{aligned}
Y_1 &= y_n, \\
\begin{cases} z_i(0) = Y_i, \\ T_i = t_n + c_i^{\{s\}}H, \\ z'_i = \Delta c_i^{\{s\}} f_s\left(T_i + \Delta c_i^{\{s\}}\theta, z_i\right), \\ Y_{i+1} = z_i(H), \end{cases} & \quad \text{for } \theta \in [0, H], \quad i = 1, \dots, s^{\{s\}}, \\
y_{n+1} &= Y_{s^{\{s\}}+1}.
\end{aligned}$$

This is simply the original ODE (1.1) solved between the abscissae of a Runge–Kutta method. With the infinitesimal step assumption, the error is zero. At the other extreme, take the surrogate model to be $f_s(t, y_s) = 0_s$. Again, (3.4) can be simplified,

but now into a traditional, unpartitioned Runge–Kutta method:

$$\begin{aligned} Y_1 &= y_n, \\ \begin{cases} T_i = t_n + c_i^{\{s\}} H, \\ Y_{i+1} = Y_i + H \sum_{j=1}^i \bar{\gamma}_{i,j} f(T_j, Y_j), \end{cases} & i = 1, \dots, s^{\{s\}}, \\ y_{n+1} &= Y_{s^{\{s\}}+1}. \end{aligned}$$

This error will be nonzero in general and can be analyzed using classical Runge–Kutta order condition and convergence theory.

While neither of these two choices for the surrogate model are particularly interesting, they illustrate how the accuracy of SM-MRI-GARK and SM-SPC-MRI-GARK depends on several factors including the accuracy of the surrogate model, the projection matrices V and W , and the method coefficients. In this section, we analyze the structure of local truncation error

$$e_{n+1} = y(t_{n+1}) - y_{n+1} = CH^{p+1} + \mathcal{O}(H^{p+2})$$

to better understand the influence of these factors. To simplify our error analysis, we use the autonomous form of (1.4), which comes at no loss of generality for internally consistent methods.

The new families of methods in this paper are derived as special cases of MRI-GARK and SPC-MRI-GARK. Interestingly, it is also possible to view MRI-GARK and SPC-MRI-GARK as special cases of the surrogate model methods. When

$$V = W^* = I_{N \times N}, \quad f(t, y) = f^{\{f\}}(t, y) + f^{\{s\}}(t, y), \quad f_s(t, y) = f^{\{f\}}(t, y),$$

we identically recover (2.2) and (2.4). Thanks to these properties, MRI-GARK and SPC-MRI-GARK order conditions are both necessary and sufficient for the surrogate model versions. Interested readers can refer to [49, Section 3.1] and [45, Section 2.2] for these order conditions, which are derived using N-tree theory [4]. Thus, the order of the surrogate model based integration only depends on the coefficients of the underlying MRI-GARK method. Assuming that f_s is sufficiently smooth and has a moderate Lipschitz constant, one can use *any* surrogate model, even a very inaccurate one, without concern of order reduction.

We turn now to the leading error constant C . N-Trees provide an elegant way to precisely determine its value. For our multirate methods, there are two partitions, so we use the set of two-trees T_2 . Tree vertices are “colored” either fast (black circle) or slow (white circle). We define the set of trees in T_2 with all fast-colored vertices as $T_2^{\{f\}}$. Now we have that

$$(4.1) \quad \begin{aligned} C &= \sum_{\substack{u \in U \\ \rho(u)=p+1}} \frac{1}{\sigma(u)} \left(\Phi(u) - \frac{1}{\gamma(u)} \right) F(u)(y), \\ U = T_2 \setminus T_2^{\{f\}} &= \left\{ \emptyset, \circ, \circ\circ, \circ\bullet, \bullet\circ, \circ\circ\circ, \circ\circ\bullet, \bullet\circ\circ, \circ\bullet\bullet, \bullet\circ\bullet, \circ\bullet\circ, \bullet\bullet\circ, \bullet\bullet\bullet, \circ\circ\circ\circ, \dots \right\} \end{aligned}$$

where $\rho(u)$, $\sigma(u)$, $\gamma(u)$, are the order, symmetries, and density, respectively [4]. The elementary weight $\Phi(u)$ depends only on the method and its coefficients. For $u \in T_2^{\{f\}}$,

$\Phi(u) = 1/\gamma(u)$ by the infinitesimal step assumption, which allows us to exclude this subset of trees from the summation in (4.1). Finally, the elementary differentials have the recursive definition

$$(4.2a) \quad F(\emptyset)(y) = y,$$

$$(4.2b) \quad F(\tau^{\{f\}})(y) = Vf_s(W^*y),$$

$$(4.2c) \quad F(\tau^{\{s\}})(y) = f(y) - Vf_s(W^*y),$$

$$(4.2d) \quad F([u_1, \dots, u_m]^{\{f\}})(y) = V \left(f_s^{(m)}(W^*y)(W^*F(u_1)(y), \dots, W^*F(u_m)(y)) \right),$$

$$(4.2e) \quad F([u_1, \dots, u_m]^{\{s\}})(y) = f^{(m)}(y)(F(u_1)(y), \dots, F(u_m)(y)) - F([u_1, \dots, u_m]^{\{f\}})(y),$$

where $\tau^{\{\sigma\}}$ is the tree with a single vertex of color $\sigma \in \{f, s\}$. A tree $u \in T_2$ can be expressed as $[u_1, \dots, u_m]^{\{\sigma\}}$ where σ is the color of the root vertex and u_1, \dots, u_m are the nonempty subtrees left when the root is removed. Table 1 provides examples of terms appearing in (4.1).




$u \in T_2 \setminus T_2^{\{f\}}$	$F(u)(y)$	$\rho(u)$	$\sigma(u)$	$\gamma(u)$
	$f(y) - Vf_s(W^*y)$	1	1	1
	$f'(y)Vf_s(W^*y) - Vf'_s(W^*y)f_s(W^*y)$	2	1	2
	$f''(y)(f(y), f(y)) - f''(y)(f(y), Vf_s(W^*y))$	3	1	3

Table 1: Examples of trees, elementary differentials, and other tree properties.

Using (4.1), the local truncation error of SM-MRI-GARK Euler from (3.6) is

$$err_{\text{Euler}} = \frac{1}{2}(f'(y_n) - Vf'_s(W^*y)W^*)f(y_n)H^2 + \mathcal{O}(H^3).$$

Note that each tree in the summation in (4.1) contains at least one slow node. From (4.2e), a slow-colored vertex corresponds to a derivative of the surrogate model error appearing in an elementary differential. Suppose there exists an ε independent of H such that the derivatives satisfy

$$\left\| f^{(m)}(y_n)(x_1, \dots, x_k) - V \left(f_s^{(m)}(W^*y_n)(W^*x_1, \dots, W^*x_m) \right) \right\| \leq \varepsilon \|x_1\| \cdots \|x_m\|,$$

for $m = 1, \dots, p$. Here, $\|\cdot\|$ denotes an arbitrary, consistent norm. Then there must be constants $c(u), c_1, \dots, c_p$ independent of H and ε such that

$$\|C\| \leq \sum_{\substack{u \in \mathcal{U} \\ \rho(u)=p+1}} c(u) \varepsilon^{\rho^{\{s\}}(u)} \leq \sum_{i=1}^p c_i \varepsilon^i,$$

where $\rho^{\{s\}}(u)$ be the number of slow vertices in u . As we might expect, the local truncation error decreases as the error in the surrogate model and its derivatives decreases.

5. Construction of surrogate models for accelerating time integration.

This section presents several techniques to construct a surrogate model f_s and the associated linear operators V and W^* , with a computationally favorable balance of accuracy and evaluation cost.

5.1. Model order reduction. There are numerous techniques from the reduced order modeling community that may be used to generate the reduced models, including proper orthogonal decomposition [54], Krylov-subspace methods [22], reduced basis methods [35], discrete empirical interpolation method [9], and dynamic mode decomposition [52, 55]. Typically, these employ an offline phase where data from the full model is collected to produce an inexpensive reduced model, which is then used in computations. Other multi-resolution methods based on Fourier or wavelet transformation [7] could be used online to only capture coarse information about the model.

5.2. Multimesh models. Consider a numerical approach to discretize a partial differential equation (PDE) in space over a computational mesh using, for example, the finite element, difference, or volume method. A surrogate model can come from solving the PDE on a coarser mesh, or using a lower order spatial discretization. This provides an approximation to capture the “shape” of the solution that is cheaper and also enjoys a less strict Courant–Friedrichs–Lewy (CFL) condition. If the meshes are nested, W is a subset of columns of the identity matrix, and V is a sparse interpolation matrix. We note that this strategy closely resembles multigrid methods [58]. The relaxation and prolongation operators, however, have to be chosen such as $W^*V = I_{N \times N}$, which is only true when the stencils do not lose information over successive applications, such as the 1D relaxation stencil $\begin{bmatrix} 0 & 1 & 0 \end{bmatrix}$ and the 1D prolongation stencil $\begin{bmatrix} 1/2 & 1 & 1/2 \end{bmatrix}$.

5.3. Applying simplifying approximations to the full model. By linearizing, filtering, averaging, simply ignoring, or otherwise approximating certain terms in f , a computationally inexpensive f_s can be produced. As an example, consider a direct N-body simulation with a Barnes-Hut or fast multipole method used as the surrogate model. In [8, Section 6] a surrogate model of z-level ocean model is produced by a vertical averaging of barotropic velocities. In many cases, this leads to an edge case where $S = N$ and $V = W = I_{N \times N}$, leading to a surrogate model with simplified dynamics, but the same state representation.

A common approach to reducing computational costs in flow problems is Large Eddy Simulation (LES). In LES, the surrogate model responsible for evolving the mean-field solution is constructed based on low-pass filtering of space or space-time modes [6]. To model the turbulence happening on the subgrid-scale, a closure model, often in the form of a dissipative term, is added to the flow equations [47]. For problems with high Reynolds numbers, time-dependent closures [18] have been proposed that need to be integrated along the equations of the model. In such cases, the filtered equations can be regarded as the reduced system f_s while the closed model is used as f for correcting the solution. In this case the V and W^* will be the same as above.

5.4. Data-driven surrogate models. When sufficient input and output data is available, supervised learning approaches are a viable option to generate approximate models for a system. A variety of techniques have been developed, some depending on system identification and sparse dictionary learning [7, 46], others using neural networks to discover operators and right-hand-side functions [38, 39]. Patch data, both in time and space [27] have been used to train machine learning models that can reproduce crude or partial dynamics of the full system. When a cheap data-driven

surrogate is available together with a larger, more accurate, physics-based model, SM-MRI-GARK methods can provide computationally balanced integration by reducing the frequency of full model evaluations while improving the overall accuracy of the solution significantly. In such cases it could be the case that the data driven dynamics reside in the full space, $S = N$, $V = W = I_{N \times N}$, or the dynamics could reside in the dominant modes of the data, in which case $S < N$ and V and W are determined by the method.

6. Numerical experiments. In order to assess the convergence and performance properties of the new surrogate model time-steppers, we apply them to a set of four ODE systems using different types of surrogate models. The methods considered in the experiments are SM-MRI-GARK Euler from (3.6) and the four methods from Appendix A. We compare these with their base methods, which are traditional Runge–Kutta methods, when only the full or only the surrogate model is used. In all the experiments, the error is computed by comparing a numerical solution to a high-accuracy reference solution at the final time. The solution using only the surrogate model resides in the surrogate model subspace, so it is multiplied by W^* before computing error.

6.1. Quasi-geostrophic model and quadratic ROM. The quasi-geostrophic (QG) equations [12, 14–16, 28], are a well-studied set of approximations to both atmospheric and ocean flow. The QG equations have a wide range of well-studied lower dimensional approximations. For our use case, a quadratic POD-Galerkin ROM makes an excellent surrogate model.

We follow the formulations of [32, 48], and the same exact setup as utilized in [36]:

$$(6.1) \quad \begin{aligned} \omega_t + J(\psi, \omega) - \text{Ro}^{-1} \psi_x &= \text{Re}^{-1} \Delta \omega + \text{Ro}^{-1} F, \\ J(\psi, \omega) &\equiv \psi_y \omega_x - \psi_x \omega_y. \end{aligned}$$

Here ω represents the vorticity, ψ the streamfunction, $\text{Re} = 450$ the Reynolds number, and $\text{Ro} = 0.0036$ the Rossby number. The vorticity and the stream function are linear transformations of each other, with, $-\Delta \psi = \omega$. The forcing term is selected to be a symmetric double Gyre to simulate flow in the ocean [21, 32, 48]:

$$(6.2) \quad F = \sin(\pi(y - 1)).$$

The domain for the problem is $\Omega = [0, 1] \times [0, 2]$. Homogeneous Dirichlet,

$$(6.3) \quad \psi(x, y) = 0, \quad \forall (x, y) \in \partial\Omega,$$

boundary conditions are used for all time.

For the spatial discretization, a second order finite difference is performed, with the canonical Arakawa approximation [3, 26] performed on the Jacobian term, J . The domain is discretized using 63 points in the x direction and 127 points in the y direction.

Following [32], and using the method of snapshots [54], we construct basis transformation operators that capture the time-averaged dominant linear modes of the system. The basis transformations are represented by the orthogonal, in L^2 , linear operators V , and W^* , where $y_s = W^* \psi$ represents the basis transformation from streamfunction space into ROM space. Details as to how these are derived are found in [36]. As the transformations are their corresponding adjoints in L^2 space, then

it must be the case that $W^*V = I_{S \times S}$, meaning that our POD-Galerkin ROM fits perfectly into the framework.

In order to construct a reduced order model we have to optimally approximate the time derivative of the reduced order state. As (6.1) is quadratic in nature, we can construct a quadratic POD-Galerkin reduced order model, of the form

$$(6.4) \quad y'_s = f_s(y_s) = W^* f(V y_s) = b + A y_s + y_s^\top \mathcal{B} y_s,$$

where y_s is the state in the POD basis, f is the solution to the Poisson equation in (6.1), $b \in \mathbb{R}^S$ corresponds to the forcing term $\text{Ro}^{-1}F$, $A \in \mathbb{R}^{S \times S}$ corresponds to the linear term $\text{Ro}^{-1}\psi_x + \text{Re}^{-1}\Delta\omega$, and $\mathcal{B} \in \mathbb{R}^{S \times S \times S}$ corresponds to the Jacobian term $-J(\psi, \omega)$. We take S , the dimension of the reduced order state space y_s to be significantly smaller than the dimension of the space of the discretized streamfunction, n . It is known from [36] that for this specific spatial discretization, utilizing $N = 8001$ points, $S = 40$ modes corresponds to 98.1% of the total kinetic energy of the system, while $S = 80$ modes corresponds to 99.4% of the total energy, meaning that this problem should be extremely well-suited to dimensional reduction.

The timespan for which we run the system will be a ten day forecast, which for the given parameters is approximately 0.109. The ROM was built in the interpolatory regime on the test timespan using 2000 evenly-spaced snapshots.

Figure 2 shows the convergence of the QG equations with respect to a ROM. Of interest is the fact that the Reduced order model needs to be extremely accurate in order for the scheme to display any decrease in error. Additionally it is evident that the smaller internal timesteps in the GARK regime versus the SPC regime play a significant role in decreasing error.

The model and the reduced order model implementations for the following experiments have been taken from [43].

6.2. Lorenz '96 with a machine learning surrogate model. The Lorenz '96 problem [31] is given by

$$(6.5) \quad \frac{d}{dt} X_k = -X_{k-2}X_{k-1} + X_{k-1}X_{k+1} - X_k + F, \quad k = 1, 2, \dots, 40,$$

with periodic boundary conditions, and a forcing term $F = 8$. Due to its chaotic dynamics, this problem is prominently used in data assimilation and atmospheric research. Readers interested in current literature on machine learning surrogate models based on Lorenz '96 may refer to [17, 41].

In the following experiments, a neural network model with fully-connected layers was trained to approximate the right-hand-side function in (6.5). Therefore the projections are $V = W^* = I_{d \times d}$ and the trained network acts as f_s . The network consists of input and output layers and a hidden layer of dimension 80. The input and hidden layers use the softplus activation function while the output layer does not have any activations.

Similar to [31], the initial condition

$$(6.6) \quad X_i(0) = \begin{cases} 8.008 & i = 20 \\ 8 & \text{otherwise} \end{cases}, \quad i = 1, \dots, 40,$$

is propagated for 2 units of time to expel transient effects and the developed solution is used as the true initial condition. The training data is taken from 5000 equally-spaced solutions of the full model within the interval $t \in [2, 10]$ and, the convergence

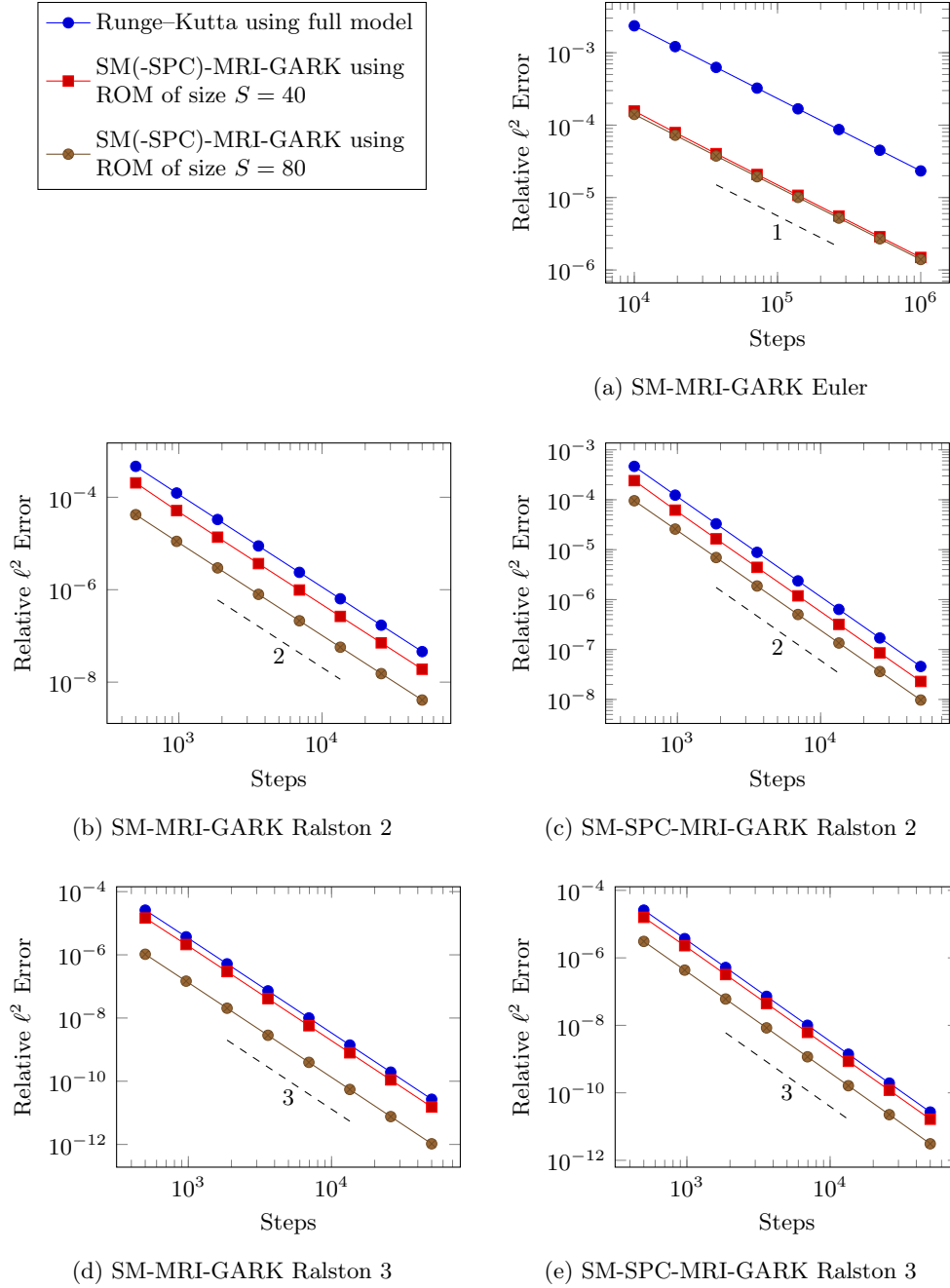


Fig. 2: Convergence plots for the Quasi-Geostrophic equations.

tests are performed over timespan $t \in [4, 8]$. The results are shown in [Figure 3](#). We note that merely integrating the surrogate model did not produce a stable solution in any of the experiments. On the other hand, when used together with the full model

in SM-MRI-GARK and SM-SPC-MRI-GARK methods, the accuracy of the solution increases significantly compared to the full model solution.

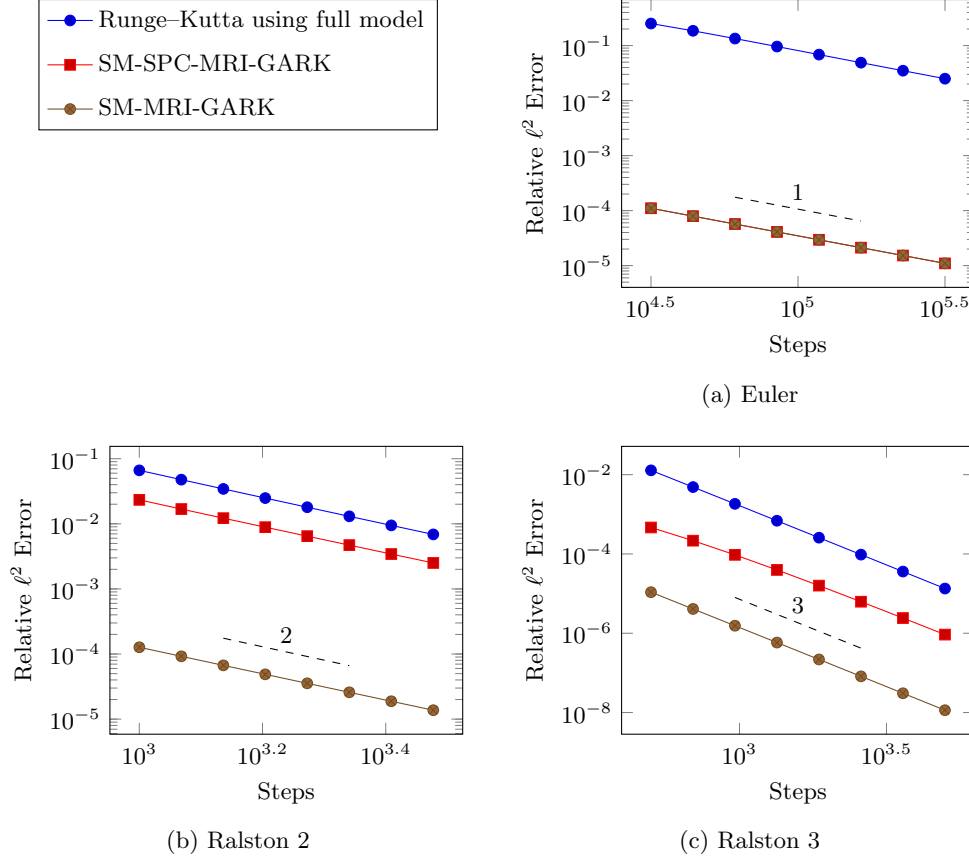


Fig. 3: Convergence plots for the Lorenz '96 problem.

6.3. Brusselator PDE. The test problem BRUS from [25, Section II.10] is based on the Brusselator reaction-diffusion PDE

$$(6.7) \quad \begin{aligned} \frac{\partial u}{\partial t} &= \alpha \nabla^2 u + 1 + u^2 v - 4.4u, \\ \frac{\partial v}{\partial t} &= \alpha \nabla^2 v + 3.4u - u^2 v, \end{aligned}$$

where $\alpha = 0.002$. The spatial domain is the unit square $0 \leq x, y \leq 1$ with zero, Neumann boundary conditions for both u and v . Using the method of lines, this is discretized with second order central finite difference on a uniform $P \times P$ grid. Starting at the initial conditions

$$u(0, x, y) = 0.5 + y, \quad v(0, x, y) = 1 + 5x,$$

we seek the solution at $t = 7.5$.

In our experiments, $P = 257$, and thus, $N = 2P^2 = 132098$. For the surrogate model, we take the approach described in [subsection 5.2](#) where we use the same finite difference discretization of [\(6.7\)](#) but on a coarser mesh. In particular, coarse meshes of size $P = 129, 65, 33$ are used, which nest inside the fine mesh. The modified fast ODEs [\(3.4b\)](#) and [\(3.7b\)](#) are solved with *one* step of a Runge–Kutta method one or two orders higher than the base method. We found that this uses the fewest evaluations of f_s while keeping the ODE solution errors negligible.

Comparing the performance of the integrators is our primary goal with the Brusselator problem, and we implemented the tests in C. For each integrator and surrogate model size, the runtime and error was recorded for a range of eight stepsizes. The results are plotted in [Figure 4](#). At orders one and two, SM-MRI-GARK and SM-SPC-MRI-GARK show clear speedups over Runge–Kutta solutions using only the full model. In addition, the performance increases as the surrogate model mesh becomes finer. Unfortunately, the results are reversed at order three. Profiling of the code helped to identify why SM-MRI-GARK and SM-SPC-MRI-GARK performed poorly. On a 129×129 grid, evaluations of f_s are about 25% as expensive as evaluation f . The linear operators V and W^* have efficient, matrix-free implementations, but are still 75% as expensive as f . These two factors caused one step of SM-MRI-GARK and SM-SPC-MRI-GARK to take approximately twice as long as a traditional Runge–Kutta step. At order three, the reduction in error is not enough to overcome this large overhead.

6.4. Advection PDE. Finally, we consider the following 2D advection problem with zero, Dirichlet boundary conditions:

$$\begin{aligned} \frac{\partial u}{\partial t} + a \cdot \nabla u &= 0, & \text{on } \Omega = [0, 1] \times [0, 1], \\ u &= 0, & \text{on } \partial\Omega. \end{aligned}$$

The velocity field is taken to be

$$a(x, y) = \begin{bmatrix} 2\pi \left(y - \frac{1}{2}\right) \\ -2\pi \left(x - \frac{1}{2}\right) \end{bmatrix},$$

which gives the so-called Molenkamp-Crowley problem. We start with the initial condition

$$u(t = 0, x, y) = \exp(-100((x - 0.35)^2 + (y - 0.35)^2))$$

and stop at $t = 2$. This allows the initial condition to rotate clockwise twice about the center of the domain.

For the method of lines discretization in space, we represent Ω with a $P \times P$ uniform, triangular mesh and apply a nodal discontinuous Galerkin (DG) method. The order in space is chosen to match the order in time. This yields the linear ODE

$$(6.8) \quad y' = M^{-1}Ky,$$

where M and K are mass and advection matrices, respectively. We use the C++ library MFEM for this DG discretization, and in particular, base it on the serial version of example 9 provided in MFEM version 4.1.

Again, we try the multimesh approach by using a mesh size of $P = 100$ for f and a mesh size of $P = 50$ for f_s . This size of the ODE [\(6.8\)](#) for each experiment is listed in [Table 2](#).

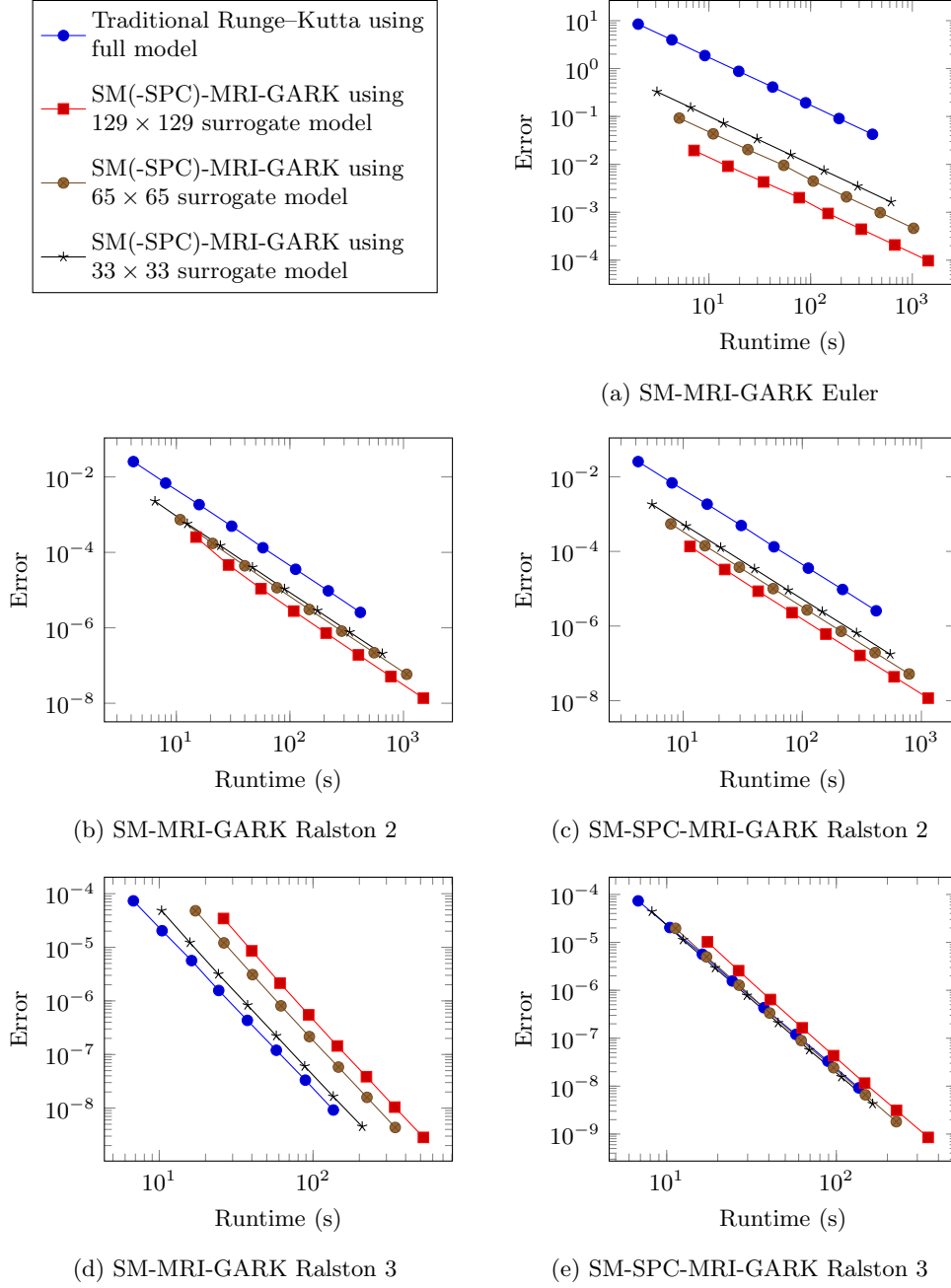


Fig. 4: Work precision diagram for BRUS.

In contrast to the Brusselator problem (6.7), the advection problem is linear and hyperbolic. Moreover, profiling reveals an evaluation of the RHS of (6.8) is much more expensive than an interpolation between meshes due, in part, to the linear solve

Order of time and space discretization	Dimension of full model N	Dimension of surrogate model S
1	6×10^4	1.5×10^4
2	1.2×10^5	3×10^4
3	2×10^5	5×10^4

Table 2: Dimensions of the full and surrogate models used in the advection experiment.

with the mass matrix. Based on the discussion in the previous subsection, we may expect better performance results at order three, and indeed, that is the case.

Figure 5 shows the error and timing for the integrators over a range of eight step-sizes. All SM-MRI-GARK and SM-SPC-MRI-GARK methods outperform Runge–Kutta methods with speedups ranging from approximately 3 to 725. The error for the Runge–Kutta methods using the surrogate model remains nearly constant, which indicates spatial errors dominate temporal errors.

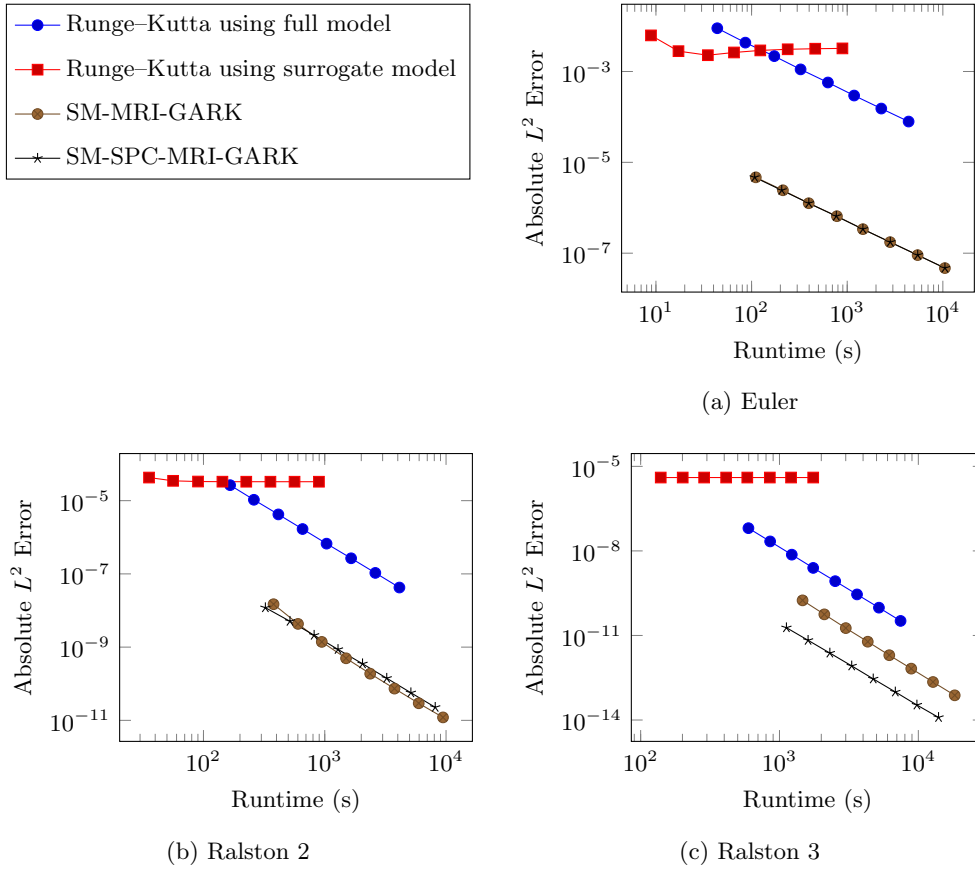


Fig. 5: Advection work precision

7. Conclusions. This work develops a new methodology to accelerate the time integration of large ODEs using surrogate models. Specifically, surrogate information is incorporated into the numerical solution of the original ODEs using multirate methods. We derive and analyze two implementations of this new time-stepping technique: SM-MRI-GARK and SM-SPC-MRI-GARK. Both combine continuous evolution of the surrogate model with discrete Runge–Kutta steps of the full ODE. There are numerous ways to generate surrogate models that offer flexible trade-offs between accuracy, computational cost, and stability. The new methods are designed such that the overall order of accuracy is independent of the surrogate model. The more accurate the surrogate models are, the smaller the error constants are, which leads to smaller local truncation errors.

Numerical experiments reveal that, at low orders of accuracy, it is possible to achieve orders of magnitude speedups versus traditional Runge–Kutta methods. As the order increases, overheads associated with evaluations of V , W^* , and the surrogate model are penalized more when measuring efficiency, and speedups tend to decrease. There is not a clear winner between SM-MRI-GARK and SM-SPC-MRI-GARK; their relative performance appears to depend heavily on the properties of the full and surrogate models.

While this paper focuses on explicit methods for nonstiff problems, the authors also plan to explore implicit methods for stiff problems and differential algebraic equations. Further extensions include applying and comparing other flavors of multirate methods for constructing surrogate model based time-steppers.

Appendix A. Explicit MRI-GARK and SPC-MRI-GARK methods of orders two and three.

Tables 3 and 4 provide coefficients for new MRI-GARK and SPC-MRI-GARK schemes based on Ralston’s optimal second and third order Runge–Kutta methods [40]. For readers interested in using different base methods or including embedded methods, we have provided a Mathematica notebook in the supplementary materials with general, parameterized families of methods.

Base Method			MRI-GARK $\Gamma(t)$	SPC-MRI-GARK $\gamma(t)$
0	0	0	$\begin{bmatrix} \frac{2}{3} & 0 \\ -\frac{5}{12} & \frac{3}{4} \end{bmatrix}$	$\begin{bmatrix} -\frac{1}{2} + \frac{3t}{2} \\ \frac{3}{2} - \frac{3t}{2} \end{bmatrix}$
$\frac{2}{3}$	$\frac{2}{3}$	0		
	$\frac{1}{4}$	$\frac{3}{4}$		

Table 3: Second order MRI-GARK and SPC-MRI-GARK coefficients.

REFERENCES

- [1] A. ABDULLE, M. J. GROTE, AND G. R. DE SOUZA, *Stabilized explicit multirate methods for stiff differential equations*, arXiv preprint arXiv:2006.00744, (2020).
- [2] J. ANDRUS, *Numerical solution for ordinary differential equations separated into subsystems*, SIAM Journal on Numerical Analysis, 16 (1979), pp. 605–611.
- [3] A. ARAKAWA, *Computational design for long-term numerical integration of the equations of fluid motion: Two-dimensional incompressible flow. Part I*, Journal of Computational Physics, 1 (1966), pp. 119–143.

Base Method				MRI-GARK $\Gamma(t)$	SPC-MRI-GARK $\gamma(t)$
0	0	0	0	$\begin{bmatrix} \frac{1}{2} & 0 & 0 \\ -\frac{11}{4} + \frac{9t}{2} & 3 - \frac{9t}{2} & 0 \\ \frac{47}{36} - \frac{13t}{6} & -\frac{1}{6} - \frac{t}{2} & -\frac{8}{9} + \frac{8t}{3} \end{bmatrix}$	$\begin{bmatrix} 1 - \frac{2t}{3} - \frac{4t^2}{3} \\ -2t + 4t^2 \\ \frac{8t}{3} - \frac{8t^2}{3} \end{bmatrix}$
$\frac{1}{2}$	$\frac{1}{2}$	0	0		
$\frac{3}{4}$	0	$\frac{3}{4}$	0		
	$\frac{2}{9}$	$\frac{1}{3}$	$\frac{4}{9}$		

Table 4: Third order MRI-GARK and SPC-MRI-GARK coefficients.

- [4] A. L. ARAÚJO, A. MURUA, AND J. M. SANZ-SERNA, *Symplectic Methods Based on Decompositions*, SIAM Journal on Numerical Analysis, 34 (1997), pp. 1926–1947, <https://doi.org/10.1137/S0036142995292128>.
- [5] T. P. BAUER AND O. KNOTH, *Extended multirate infinitesimal step methods: Derivation of order conditions*, Journal of Computational and Applied Mathematics, (2019), <https://doi.org/10.1016/j.cam.2019.112541>.
- [6] L. C. BERSELLI, T. ILIESCU, AND W. J. LAYTON, *Mathematics of large eddy simulation of turbulent flows*, Springer, Berlin New York, 2006.
- [7] S. L. BRUNTON AND J. N. KUTZ, *Data-driven science and engineering: Machine learning, dynamical systems, and control*, Cambridge University Press, 2019.
- [8] L. CHACÓN, G. CHEN, D. KNOLL, C. NEWMAN, H. PARK, W. TAITANO, J. WILLERT, AND G. WOMELDORFF, *Multiscale high-order/low-order (HOLO) algorithms and applications*, Journal of Computational Physics, 330 (2017), pp. 21 – 45, <https://doi.org/https://doi.org/10.1016/j.jcp.2016.10.069>.
- [9] S. CHATURANTABUT AND D. C. SORESENSEN, *Nonlinear model reduction via discrete empirical interpolation*, SIAM Journal on Scientific Computing, 32 (2010), pp. 2737–2764.
- [10] E. CONSTANTINESCU AND A. SANDU, *Multirate timestepping methods for hyperbolic conservation laws*, Journal on Scientific Computing, 33 (2007), pp. 239–278, <https://doi.org/10.1007/s10915-007-9151-y>, <http://dx.doi.org/10.1007/s10915-007-9151-y>.
- [11] E. CONSTANTINESCU AND A. SANDU, *Extrapolated multirate methods for differential equations with multiple time scales*, Journal of Scientific Computing, 56 (2013), pp. 28–44, <https://doi.org/10.1007/s10915-012-9662-z>, <http://dx.doi.org/10.1007/s10915-012-9662-z>.
- [12] J. FERGUSON, *A numerical solution for the barotropic vorticity equation forced by an equatorially trapped wave*, master’s thesis, University of Victoria, 2008.
- [13] A. I. FORRESTER AND A. J. KEANE, *Recent advances in surrogate-based optimization*, Progress in Aerospace Sciences, 45 (2009), pp. 50 – 79, <https://doi.org/https://doi.org/10.1016/j.paerosci.2008.11.001>.
- [14] E. L. FOSTER, T. ILIESCU, AND Z. WANG, *A finite element discretization of the streamfunction formulation of the stationary quasi-geostrophic equations of the ocean*, Comput. Methods Appl. Mech. Engrg., 261 (2013), pp. 105–117.
- [15] E. L. FOSTER, T. ILIESCU, AND D. R. WELLS, *A two-level finite element discretization of the streamfunction formulation of the stationary quasi-geostrophic equations of the ocean*, Comput. Math. Appl., 66 (2013), pp. 1261–1271.
- [16] E. L. FOSTER, T. ILIESCU, AND D. R. WELLS, *A conforming finite element discretization of the streamfunction form of the unsteady quasi-geostrophic equations*, Int. J. Numer. Anal. Mod., 13 (2016).
- [17] D. J. GAGNE, H. M. CHRISTENSEN, A. C. SUBRAMANIAN, AND A. H. MONAHAN, *Machine Learning for Stochastic Parameterization: Generative Adversarial Networks in the Lorenz ’96 Model*, Journal of Advances in Modeling Earth Systems, 12 (2020), p. e2019MS001896, <https://doi.org/10.1029/2019MS001896>.
- [18] P. GAMNITZER, V. GRAVEMEIER, AND W. A. WALL, *Time-dependent subgrid scales in residual-based large eddy simulation of turbulent channel flow*, Computer Methods in Applied Mechanics and Engineering, 199 (2010), pp. 819–827, <https://doi.org/10.1016/j.cma.2009.07.009>.
- [19] C. GEAR, *Multirate methods for ordinary differential equations*, tech. report, Illinois Univ., Urbana (USA). Dept. of Computer Science, 1974.
- [20] C. GEAR AND D. WELLS, *Multirate linear multistep methods*, BIT, 24 (1984), pp. 484–502.
- [21] R. J. GREATBATCH AND B. T. NADIGA, *Four-gyre circulation in a barotropic model with double-*

- gyre wind forcing*, J. Phys. Oceanogr., 30 (2000), pp. 1461–1471.
- [22] E. GRIMME, *Krylov projection methods for model reduction*, theses, University of Illinois at Urbana Champaign, May 1997, <https://tel.archives-ouvertes.fr/tel-01711328>.
 - [23] M. GÜNTHER AND A. SANDU, *Multirate generalized additive Runge-Kutta methods*, Numerische Mathematik, 133 (2016), pp. 497–524, <https://doi.org/10.1007/s00211-015-0756-z>, <http://dx.doi.org/10.1007/s00211-015-0756-z>.
 - [24] C. HACHTEL, J. KERLER-BACK, A. BARTEL, M. GÜNTHER, AND T. STYKEL, *Multirate DAE/ODE-simulation and model order reduction for coupled field-circuit systems*, in Scientific Computing in Electrical Engineering, U. Langer, W. Amrhein, and W. Zulehner, eds., Cham, 2018, Springer International Publishing, pp. 91–100.
 - [25] E. HAIRER, S. P. NØRSETT, AND G. WANNER, *Solving Ordinary Differential Equations I: Non-stiff Problems*, vol. 8 of Springer Series in Computational Mathematics, Springer-Verlag, Berlin, Heidelberg, 2nd ed., 1993, <https://doi.org/10.1007/978-3-540-78862-1>.
 - [26] D. C. JESPERSEN, *Arakawa’s method is a finite-element method*, Journal of computational physics, 16 (1974), pp. 383–390.
 - [27] I. G. KEVREKIDIS, C. W. GEAR, AND G. HUMMER, *Equation-free: The computer-aided analysis of complex multiscale systems*, AIChE Journal, 50 (2004), pp. 1346–1355, <https://doi.org/10.1002/aic.10106>.
 - [28] T. Y. KIM, E. FRIED, AND T. ILIESCU, *B-spline based finite-element method for the stationary quasi-geostrophic equations of the ocean*, Comput. Meth. Appl. Mech. Eng., 286 (2015), pp. 168–191.
 - [29] O. KNOTH AND R. WOLKE, *Implicit-explicit Runge-Kutta methods for computing atmospheric reactive flows*, Applied Numerical Mathematics, 28 (1998).
 - [30] P. J. LANZKRON, D. J. ROSE, AND J. T. WILKES, *An analysis of approximate nonlinear elimination*, SIAM Journal on Scientific Computing, 17 (1996), pp. 538–559, <https://doi.org/10.1137/S106482759325154X>.
 - [31] E. N. LORENZ, *Predictability: A problem partly solved*, in Proc. Seminar on predictability, vol. 1, 1996.
 - [32] C. MOU, H. LIU, D. R. WELLS, AND T. ILIESCU, *Data-driven correction reduced order models for the quasi-geostrophic equations: A numerical investigation*, arXiv preprint, <http://arxiv.org/abs/1908.05297>, (2019).
 - [33] M. NARAYANAMURTHI, P. TRANQUILLI, A. SANDU, AND M. TOKMAN, *EPIRK-W and EPIRK-K time integration methods*, Journal of Scientific Computing, 78 (2019), pp. 167–201, <https://doi.org/10.1007/s10915-018-0761-3>, <https://doi.org/10.1007/s10915-018-0761-3>.
 - [34] Y. S. ONG, P. B. NAIR, AND A. J. KEANE, *Evolutionary optimization of computationally expensive problems via surrogate modeling*, AIAA Journal, 41 (2003), pp. 687–696, <https://doi.org/10.2514/2.1999>.
 - [35] J. S. PETERSON, *The reduced basis method for incompressible viscous flow calculations*, SIAM Journal on Scientific and Statistical Computing, 10 (1989), pp. 777–786.
 - [36] A. A. POPOV, C. MOU, T. ILIESCU, AND A. SANDU, *A multifidelity ensemble Kalman filter with reduced order control variates*, SIAM Journal of Scientific Computing, submitted (2020).
 - [37] N. V. QUEIPO, R. T. HAFTKA, W. SHYY, T. GOEL, R. VAIDYANATHAN, AND P. KEVIN TUCKER, *Surrogate-based analysis and optimization*, Progress in Aerospace Sciences, 41 (2005), pp. 1 – 28, <https://doi.org/https://doi.org/10.1016/j.paerosci.2005.02.001>.
 - [38] M. RAISSI, P. PERDIKARIS, AND G. E. KARNIADAKIS, *Numerical Gaussian Processes for Time-Dependent and Nonlinear Partial Differential Equations*, SIAM Journal on Scientific Computing, (2018).
 - [39] M. RAISSI, P. PERDIKARIS, AND G. E. KARNIADAKIS, *Physics-informed neural networks: A deep learning framework for solving forward and inverse problems involving nonlinear partial differential equations*, Journal of Computational Physics, 378 (2019), pp. 686–707, <https://doi.org/10.1016/j.jcp.2018.10.045>.
 - [40] A. RALSTON, *Runge-Kutta methods with minimum error bounds*, Mathematics of computation, 16 (1962), pp. 431–437.
 - [41] S. RASP, *Coupled online learning as a way to tackle instabilities and biases in neural network parameterizations: general algorithms and Lorenz 96 case study (v1.0)*, Geoscientific Model Development, 13 (2020), pp. 2185–2196, <https://doi.org/10.5194/gmd-13-2185-2020>.
 - [42] J. RICE, *Split Runge-Kutta methods for simultaneous equations*, Journal of Research of the National Institute of Standards and Technology, 60 (1960).
 - [43] S. ROBERTS, A. A. POPOV, AND A. SANDU, *ODE test problems: a MATLAB suite of initial value problems*, Tech. Report CSL-TR-19-1, Computational Science Laboratory, Virginia Tech, 2019, <https://doi.org/arXiv:1901.04098>, <https://github.com/ComputationalScienceLaboratory/ODE-Test-Problems>.

- [44] S. ROBERTS, A. SARSHAR, AND A. SANDU, *Coupled multirate infinitesimal GARK methods for stiff differential equations with multiple time scales*, SIAM Journal on Scientific Computing, 42 (2020), pp. A1609–A1638, <https://doi.org/10.1137/19M1266952>, <https://arxiv.org/abs/1808.02759>.
- [45] S. ROBERTS, A. SARSHAR, AND A. SANDU, *Coupled multirate infinitesimal GARK schemes for stiff systems with multiple time scales*, SIAM Journal on Scientific Computing, 42 (2020), pp. A1609–A1638, <https://doi.org/10.1137/19M1266952>.
- [46] S. H. RUDY, S. L. BRUNTON, J. L. PROCTOR, AND J. N. KUTZ, *Data-driven discovery of partial differential equations*, Science Advances, 3 (2017), p. e1602614, <https://doi.org/10.1126/sciadv.1602614>.
- [47] P. SAGAUT, *Large eddy simulation for incompressible flows: an introduction*, Springer Science & Business Media, 2006.
- [48] O. SAN AND T. ILIESCU, *A stabilized proper orthogonal decomposition reduced-order model for large scale quasigeostrophic ocean circulation*, Advances in Computational Mathematics, 41 (2015), pp. 1289–1319.
- [49] A. SANDU, *A class of multirate infinitesimal GARK methods*, SIAM Journal on Numerical Analysis, 57 (2019), pp. 2300–2327, <https://doi.org/10.1137/18M1205492>, <https://doi.org/10.1137/18M1205492>.
- [50] A. SANDU AND E. CONSTANTINESCU, *Multirate Adams methods for hyperbolic equations*, Journal of Scientific Computing, 38 (2009), pp. 229–249, <https://doi.org/doi:10.1007/s10915-008-9235-3>, <http://dx.doi.org/10.1007/s10915-008-9235-3>.
- [51] A. SARSHAR, S. ROBERTS, AND A. SANDU, *Design of high-order decoupled multirate GARK schemes*, SIAM Journal on Scientific Computing, 41 (2019), pp. A816–A847, <https://doi.org/10.1137/18M1182875>, <https://doi.org/10.1137/18M1182875>.
- [52] P. J. SCHMID, *Dynamic mode decomposition of numerical and experimental data*, Journal of fluid mechanics, 656 (2010), pp. 5–28.
- [53] J. M. SEXTON AND D. R. REYNOLDS, *Relaxed multirate infinitesimal step methods*, arXiv preprint arXiv:1808.03718, (2018). Submitted to J. Comput. Appl. Math.
- [54] L. SIROVICH, *Turbulence and the dynamics of coherent structures part I: Coherent structures*, Quarterly of applied mathematics, 45 (1987), pp. 561–571.
- [55] G. TISSOT, L. CORDIER, N. BENARD, AND B. R. NOACK, *Model reduction using dynamic mode decomposition*, Comptes Rendus Mécanique, 342 (2014), pp. 410–416.
- [56] M. TOKMAN, *A new class of exponential propagation iterative methods of Runge–Kutta type (EPIRK)*, Journal of Computational Physics, 230 (2011), pp. 8762–8778.
- [57] J. WENSCH, O. KNOTH, AND A. GALANT, *Multirate infinitesimal step methods for atmospheric flow simulation*, BIT Numerical Mathematics, 49 (2009), pp. 449–473.
- [58] H. B. ZUBAIR, *Efficient Multigrid Methods based on Improved Coarse Grid Correction Techniques.*, PhD thesis, Delft University of Technology, Netherlands, 2009.